JACS
JOURNAL OF THE AMERICAN CHEMICAL SOCIETY
Communication
pubs.acs.org/JACS

Reversible O–O Bond Scission of Peroxodiiron(III) to High-Spin Oxodiiron(IV) in Dioxygen Activation of a Diiron Center with a Bis-tpa Dinucleating Ligand as a Soluble Methane Monooxygenase Model

Masahito Kodera,*[,†] Yuka Kawahara,[†] Yutaka Hitomi,[†] Takashi Nomura,[‡] Takashi Ogura,[‡] and Yoshio Kobayashi[§]

[†]Department of Molecular Chemistry and Biochemistry, Doshisha University, Tatara Miyakotani 1-3, Kyotanabe, Kyoto 610-0321, Japan

[‡]Department of Life Science, University of Hyogo, Kouto 2-1, Ako-gun Kamigori-cho, Hyogo 678-1297, Japan

[§]Nishina Center, The Institute for Physical and Chemical Research (RIKEN), Hirosawa 3-2-1, Wako, Saitama 351-0198, Japan

Supporting Information

ABSTRACT: The conversion of peroxodiiron(III) to high-spin S = 2 oxodiiron(IV) via reversible O–O bond scission in a diiron complex with a bis-tpa dinucleating ligand, 6-hpa, has been characterized by elemental analysis; kinetic measurements for alkene epoxidation; cold-spray ionization mass spectrometry; and electronic absorption, Mössbauer, and resonance Raman spectroscopy to gain insight into the O_2 activation mechanism of soluble methane monooxygenases. This is the first synthetic example of a high-spin S = 2 oxodiiron(IV) species that oxidizes alkenes to epoxides efficiently. The bistability of the peroxodiiron(III) and high-spin S = 2 oxodiiron(IV) moieties is the key feature for the reversible O–O bond scission.

Soluble methane monooxygenases (sMMOs) are non-heme diiron enzymes that catalyze the conversion of CH_4 to CH_3OH, one of the most difficult chemical oxidations, via dioxygen activation. In this process, the intermediate P, a peroxodiiron(III) generated by binding of O_2 to diiron(II), is converted to the active species Q, an oxodiiron(IV), which is responsible for the CH_4 oxidation.[1−3] The diiron(IV) of Q is in a high-spin S = 2 state.[3] A di-μ-oxodiiron(IV) diamond core structure has been proposed for Q on the basis of the short Fe···Fe distance (2.5 Å)[4] but has not been established. The conversion of P to Q, however, has not been clarified because of their instability.[3,5] Thus, a functional model attaining conversion of peroxodiiron(III) to high-spin oxodiiron(IV) would be useful for clarification of the P-to-Q conversion mechanism.

To date, only a few oxodiiron(IV) complexes have been reported. The crystal structure of a μ-oxodiiron(IV) complex with the macrocyclic tetraamidate ligand (TAML), $(PPh_4)_2[Fe_2(\mu\text{-}O)(TAML)_2]$ (**1**), was determined by Collins.[6] Que reported the di-μ-oxodiiron(IV) complex $[Fe_2(\mu\text{-}O)_2(L)_2]^{4+}$ (**2a**)[7] and the μ-oxo-oxohydroxodiiron(IV) complex $[Fe_2(\mu\text{-}O)(O)(OH)(L)_2]^{3+}$ (**2b**)[8] [L = tris(3,5-dimethyl-4-methoxypyridin-2-ylmethyl)amine], where **2a** forms the diamond core structure and **2b** mimics the P-to-Q conversion of sMMO. These complexes, however, are in a low-spin S = 1 state, different from the high-spin S = 2 state of Q, and are converted to mononuclear complexes in solution because the supporting ligands do not stabilize a dinuclear structure.[6,7] Meanwhile, we reported predominant epoxidation of alkenes with H_2O_2 catalyzed by $[Fe_2(\mu\text{-}O)(OH_2)_2(6\text{-hpa})](ClO_4)_4$ (**3**),[9] in which 6-hpa is 1,2-bis{2-[bis(2-pyridylmethyl)-aminomethyl]pyridin-6-yl}ethane. The chemical structure of 6-hpa is shown in Scheme 1. The μ-oxodiiron structure of **3** is essential for the predominant epoxidation, sMMO-like reactivity. Detailed isotope-labeling experiments and spectral pursuits for the reaction of **3** with H_2O_2 suggested the generation of a μ-oxodioxodiiron(IV) as the active species and scrambling of the three O atoms in it.

Scheme 1. Chemical Structure of 6-hpa

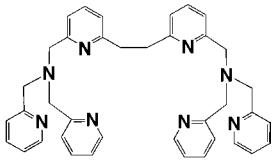

We report herein the spectroscopic characterization of two reaction intermediates generated from **3** upon reaction with H_2O_2: the μ-oxo-μ-peroxodiiron(III) complex $[Fe_2(\mu\text{-}O)(\mu\text{-}O_2)(6\text{-hpa})](ClO_4)_2$ (**4a**) and the μ-oxodioxodiiron(IV) complex $[Fe_2(\mu\text{-}O)(O)_2(6\text{-hpa})](ClO_4)_2$ (**4b**). The transformation of **3** to **4a** and **4b** is shown in Scheme 2.

Addition of 1.2 equiv of H_2O_2 to a solution of **3** in the presence of 2 equiv of Et_3N (necessary for deprotonation) in MeCN under N_2 at −40 °C generated a new species, **4**, that exhibits absorption bands at 500 nm (ε = 1092 M^{-1} cm^{-1}), 610 (821), and 783 (204) [Figure S1 in the Supporting Information (SI)]. These are similar to absorption bands at 494 nm (ε = 1100 M^{-1} cm^{-1}), 648 (1200), and 846 (230) reported for the

Received: June 22, 2012
Published: July 28, 2012

dx.doi.org/10.1021/ja306089q | J. Am. Chem. Soc. 2012, 134, 13236−13239

Scheme 2. Transformation of 3 to μ-Oxo-μ-peroxodiiron(III) Complex 4a and μ-Oxodioxodiiron(IV) Complex 4b

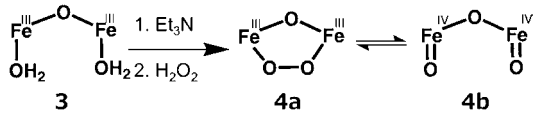

μ-oxo-μ-peroxodiiron(III) complex $[Fe_2(\mu\text{-}O)(\mu\text{-}O_2)(6\text{-}Me_3\text{-}tpa)_2](ClO_4)_2$ (**5**),[10] although there are some differences, suggesting that **4** partly contains a similar peroxo complex. **4** is stable at −40 °C, so kinetic studies were carried out at −30 °C. The spontaneous decomposition of **4** obeyed first-order kinetics with $k = 1.3 \times 10^{-3}$ s^{-1} at −30 °C, and the plot of ln[**4**] versus t remained linear for 4 half-lives. The decay rate of **4** was sensitive to the concentration of *trans*-β-methylstyrene as a substrate (see the SI). The kinetic results indicated that **4** acts as a direct oxidant. **4** is ESR-silent, implying the presence of a μ-oxo bridge that causes an antiferromagnetic interaction between the two Fe ions.[34] The cold-spray ionization mass spectrum of **4** showed a major peak at m/z 865, corresponding to $\{[Fe_2O_3(6\text{-hpa})](ClO_4)\}^+$ (Figure S2). Moreover, **4** was isolated as green solid in 93% yield (based on **3**) upon addition of Et_2O at −40 °C. Thus, the conversion of **3** to **4** is quantitative because the diiron core is stabilized by the dinucleating 6-hpa ligand. Elemental analysis of **4** agreed with a formula $[Fe_2O_3(6\text{-hpa})](ClO_4)_2{\cdot}4H_2O$ within 0.3% error (see the SI). The isolated **4** reacted with *trans*-β-methylstyrene to give the epoxide in 86% yield. All of the results shown here suggested that upon reaction of **3** with H_2O_2 in the presence of Et_3N, a μ-oxo-μ-peroxodiiron(III) complex is produced and easily converted to an active species having the same molecular formula. Thus, **4** may be a mixture of the peroxo intermediate **4a** and the active species **4b**, as shown in Scheme 2.

Mössbauer spectra of the isolated solid **4** were recorded between 25 and 295 K at zero field. The spectrum at 25 K is composed of two quadrupole doublets with $\delta = 0.351(3)$ mm/s, $\Delta E_Q = 1.635(5)$ mm/s and $\delta = 0.132(9)$ mm/s, $\Delta E_Q = 0.438(2)$ mm/s, as shown by the deconvolution spectra (red and blue lines, respectively, in Figure 1a). The isomer shift (δ) and quadrupole splitting (ΔE_Q) for the red line are close to the corresponding values of 0.54 and 1.68 mm/s, respectively, for μ-oxo-μ-peroxodiiron(III) complex **5**,[10] 0.66 and 1.40 mm/s for a μ-peroxo-di-μ-benzoatodiiron(III) complex with the sterically hindered trispyrazolylborate ligand $HB(pz')_3$,[11] and 0.53 and 1.68 mm/s for a μ-peroxo-di-μ-acetatodiiron(III) complex with the hexpy ligand.[12] Thus, the red line may result from a diiron(III) moiety symmetrically bridged by the peroxide. The δ and ΔE_Q values for the blue line are close to the values $\delta = 0.14$−0.21 mm/s and $\Delta E_Q = 0.53$−0.68 mm/s for the high-spin $S = 2$ diiron(IV) moiety in the active species Q of sMMO.[3,5,13−15] The high-spin $S = 2$ iron(IV) complexes reported to date show δ and ΔE_Q values of ∼0.1 and ∼0.5 mm/s,[16−19] respectively, but low-spin $S = 1$ iron(IV) complexes exhibit relatively higher ΔE_Q values of 1−2 mm/s.[14] Thus, the blue line must be due to a high-spin $S = 2$ diiron(IV) species with a symmetric structure. These results and all of the other spectral and analytical data shown above demonstrated that **4** is composed of the μ-oxo-μ-peroxodiiron(III) complex **4a** and the high-spin $S = 2$ μ-oxodioxodiiron(IV) complex **4b**. Here, **4b** is the first synthetic example of a high-spin $S = 2$ oxodiiron(IV) complex.

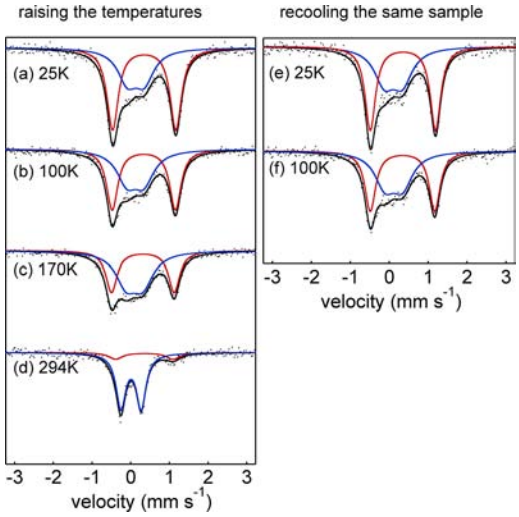

Figure 1. Zero-field Mössbauer spectra of **4** recorded when the temperature was raised to (a) 25, (b) 100, (c) 170, and (d) 294 K and, after recooling of the same sample, at (e) 25 and (f) 100 K. Black lines are the least-squares fits to the raw data, and the red and blue lines are the deconvolution spectra corresponding to μ-oxo-μ-peroxodiiron(III) complex **4a** and μ-oxo-dioxodiiron(IV) complex **4b**.

The most interesting feature, the reversible conversion between **4a** and **4b**, was observed by temperature-dependent Mössbauer spectra. As shown in Figure 1a−d, raising the temperature from 25 to 295 K decreased the amount of **4a** and increased the amount of **4b**. The **4a**:**4b** ratios estimated from the deconvolution spectra were 61:39, 53:47, 31:69, and 15:85 at 25, 100, 170, and 295 K, respectively. After these measurements, the same sample was cooled again, and Mössbauer spectra were recorded at 25 and 100 K (Figure 1e,f). The **4a**:**4b** ratios in Figure 1e,f are almost equal to those obtained for the first measurements shown in Figure 1a,b, respectively, demonstrating that **4a** and **4b** are reversibly interconverted. In the reversible conversion, homolytic O−O bond scission of **4a** and rebinding of the resultant two O atoms in the terminal Fe(IV)═O moieties of **4b** must occur (see Scheme 2). Therefore, this is the first spectroscopic observation of dioxygen activation via reversible O−O bond scission of a peroxodiiron(III) to a high-spin $S = 2$ oxodiiron(IV), and this serves as a functional model for the conversion of P to Q in the O_2 activation of sMMOs.

The terminal Fe(IV)═O moieties of **4b** were detected by resonance Raman measurements. The spectrum of **4** (generated as shown above with $H_2{}^{16}O_2$ in MeCN at −40 °C) was obtained with 607 nm excitation and showed a band at 820 cm^{-1} (Figure 2A, spectrum a), which shifted to 777 cm^{-1} (Figure 2A, spectrum b) when **4** was labeled using $H_2{}^{18}O_2$. The band at 820 cm^{-1} can be assigned to the Fe−O stretching vibration of the terminal Fe(IV)═O moieties of **4b** because it is in the range of 798−843 cm^{-1} reported for Fe−O stretches of Fe(IV)═O complexes.[16,18,20−23] The observed isotope shift of 43 cm^{-1} is slightly larger than the value of 36 cm^{-1} expected on the basis of an Fe−O harmonic oscillator model. This may be explained by coupling with the Fe(IV)−O−Fe(IV) moiety, as a similar isotope shift of 46 cm^{-1} was reported for the stretching vibration of the terminal Fe(IV)═O moiety in an Fe(III)−O−Fe(IV)═O dinuclear complex with the 6-Me_3-tpa ligand.[24] The O−O stretching vibration of **4a** could not be clearly detected in the range of 822−919 cm^{-1} reported for μ-

dx.doi.org/10.1021/ja306089q | J. Am. Chem. Soc. 2012, 134, 13236−13239

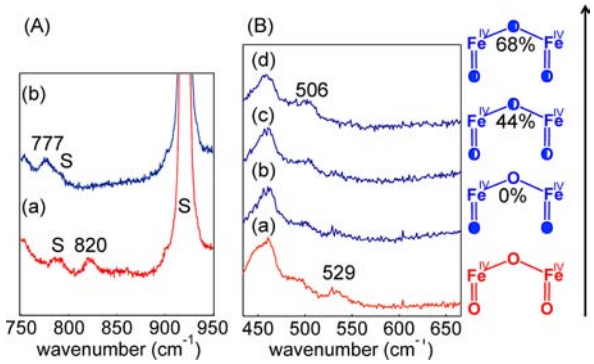

Figure 2. Resonance Raman spectra of **4** in MeCN at −40 °C obtained with excitation at (A) 607 and (B) 407 nm. The samples were prepared by treating **3** with 2 equiv of $H_2{}^{16}O_2$ (red lines) or $H_2{}^{18}O_2$ (blue lines) in the presence of 2 equiv of Et_3N in MeCN at −40 °C. In (B), spectra b−d were recorded at intervals of 200 s. The numbers shown in the spectra are the corresponding vibrational bands of **4b**. "S" labels indicate solvent bands. The diagram at the right shows schematic drawings of **4b** corresponding to spectra a−d in (B), in which the numbers are the percentages of ^{18}O incorporation into the μ-oxo bridges.

peroxodiiron(III) complexes.[25−28,31] Under the resonance Raman conditions, **4a** is the minor component, as the **4a**:**4b** ratio at −40 °C was estimated to be 25:75 by temperature-dependent Mössbauer measurements (Figure S3). This may be the reason that the O−O band was not clearly detected.

As a dynamic behavior of **4b**, we previously proposed the scrambling of the three O atoms in the μ-oxodioxodiiron(IV) core. Here we directly observed it in the resonance Raman spectra by monitoring the Fe(IV)−O−Fe(IV) symmetric stretching vibration, ν_s{Fe(IV)−O−Fe(IV)}, upon 407 nm excitation of the oxodimer region,[29] as shown in Figure 2B. **4b** was generated with 2 equiv of $H_2{}^{16}O_2$ (Figure 2B, spectrum a) or $H_2{}^{18}O_2$ (Figure 2B, spectra b−d). Spectrum a in Figure 2B shows a clear band at 529 cm^{-1} that is assignable to ν_s{Fe(IV)−^{16}O−Fe(IV)} because μ-oxodiiron complexes generally exhibit a strongly enhanced Fe−O−Fe symmetric stretching vibration in the resonance Raman spectrum upon excitation into an oxodimer region.[30] When **4b** was labeled ^{18}O using $H_2{}^{18}O_2$, the spectra (b−d in Figure 2B) were recorded at intervals of 200 s. Spectrum b in Figure 2B, obtained just after addition of $H_2{}^{18}O_2$, showed a major band at 529 cm^{-1} and a minor one at 506 cm^{-1}. The former results from ν_s{Fe(IV)−^{16}O−Fe(IV)}, and the latter can be assigned to ν_s{Fe(IV)−^{18}O−Fe(IV)} on the basis of the Fe−O harmonic oscillator model, which predicts a difference of 23 cm^{-1} between the ^{16}O and ^{18}O isotopomers. The former peak gradually decreased and the latter increased (Figure 2B, spectrum c). Finally, in Figure 2 B, spectrum d, the former peak almost disappeared and the latter one became the major peak. These time-dependent spectral changes can be explained by scrambling of the three O atoms in the μ-oxodioxodiiron(IV) core of **4b**, where the ^{16}O atom of the μ-oxo bridge is exchanged with the ^{18}O atoms of the two terminal Fe(IV)=^{18}O moieties; theoretically, 89% of the μ-oxo bridge should be ^{18}O-labeled after consumption of 2 equiv of $H_2{}^{18}O_2$. The observed percentage of ^{18}O incorporation into the μ-oxo-O atom of **4b** was estimated from the integrated intensity ratio of the Raman bands at 529 and 506 cm^{-1} for each spectrum shown in Figure 2B; the estimated values of 0, 44, and 68% are shown. The estimation method is shown in Figure S8. This demonstrated that the scrambling easily occurs even at −40 °C. Thus, the scrambling may be the intrinsic dynamic behavior in the μ-oxodioxodiiron(IV) core of **4b**.

The characterization of $[Fe^{III}{}_2(\mu\text{-O})(\mu\text{-O}_2)(6\text{-hpa})](ClO_4)_2$ (**4a**) and $[Fe^{IV}{}_2(\mu\text{-O})(O)_2(6\text{-hpa})](ClO_4)_2$ (**4b**) allowed us to clarify for the first time dioxygen activation via reversible O−O bond scission on the diiron center. To date, many peroxodiiron(III) complexes[31] and only a few oxodiiron(IV) complexes[6−8] have been reported, but in their synthetic compounds, usually only either the peroxodiiron(III) or oxodiiron(IV) is stabilized. Meanwhile, sMMOs generate some intermediates involving P and Q in the dioxygen activation, where the conformational change around the diiron center may play an essential role in stabilizing them and controlling the conversion.[32] By using the dinucleating ligand 6-hpa, we succeeded in stabilizing both the peroxodiiron(III) complex **4a** and the oxodiiron(IV) complex **4b**. Thus, the bistability of **4a** and **4b** is the reason why the reversible O−O bond scission was observed and must make the conversion between them easier. In this system, **4b** is the major component at 294 K on the basis of the component ratio of 85% estimated from the Mössbauer spectra, leading to efficient alkene epoxidation at room temperature. Therefore, it may be concluded that the bistability is effective in reducing the energy barrier of the dioxygen activation, control of which is essential for the efficient catalysis of substrate oxidation.

Moreover, in **4b**, the diiron(IV) is in a high-spin $S = 2$ state. To date, no examples of a synthetic oxodiiron(IV) complex in a high-spin $S = 2$ state have been reported. In high-valence iron(IV), a high-spin $S = 2$ state is generally less stable than a low-spin $S = 1$ state.[33] Thus, the high-spin state of **4b** is metastable, and the bistability of **4a** and **4b** may make it possible. In enzyme systems, reaction intermediates must be metastable.[35] That is why enzymatic reactions proceed smoothly. On the contrary, the most stable state is a kind of dead end of the reaction. The most important thing, however, is that it is not chemically understood how the high-spin $S = 2$ state of the oxodiiron(IV) active species Q is attained in sMMOs. Therefore, further detailed structural studies of **4a** and **4b** may be needed to gain some insight into the structural reasons for stabilization of the high-spin $S = 2$ oxodiiron(IV) in the active species Q of sMMO.

■ ASSOCIATED CONTENT

Ⓢ Supporting Information

Experimental details of synthesis and isolation, spectral data, and kinetic measurements of **4** are included. This material is available free of charge via the Internet at http://pubs.acs.org.

■ AUTHOR INFORMATION

Corresponding Author

mkodera@mail.doshisha.ac.jp.

Notes

The authors declare no competing financial interest.

■ ACKNOWLEDGMENTS

This work was supported by a Grant-in-Aid for Scientific Research B (21350037) from the Ministry of Education, Culture, Sports, Science and Technology (MEXT), Japan, and by "Creating Research Center for Advanced Molecular Biochemistry", Strategic Development of Research Infrastructure for Private Universities, from MEXT.

REFERENCES

(1) Tinberg, C. E.; Lippard, S. J. *Acc. Chem. Res.* **2011**, *44*, 280−288.
(2) Friedle, S.; Reisner, E.; Lippard, S. J. *Chem. Soc. Rev.* **2010**, *39*, 2768−2779.
(3) Wallar, B. J.; Lipscomb, J. D. *Chem. Rev.* **1996**, *96*, 2625−2658.
(4) Shu, L.; Nesheim, J. C.; Kauffmann, K.; Münck, E.; Lipscomb, J. D.; Que, L., Jr. *Science* **1997**, *275*, 515−518.
(5) Liu, K. E.; Valentine, A. M.; Wang, D.; Huynh, B. H.; Edmondson, D. E.; Salifoglou, A.; Lippard, S. J. *J. Am. Chem. Soc.* **1995**, *117*, 10174−10185.
(6) Ghosh, A.; Tiago De Oliveira, F.; Yano, T.; Nishioka, T.; Beach, E. S.; Kinoshita, I.; Münck, E.; Ryabov, A. D.; Horwitz, C. P.; Collins, T. J. *J. Am. Chem. Soc.* **2005**, *127*, 2505−2513.
(7) Xue, G.; Wang, D.; De Hont, R.; Fiedler, A. T.; Shan, X.; Münck, E.; Que, L., Jr. *Proc. Natl. Acad. Sci. U.S.A.* **2007**, *104*, 20713−20718.
(8) Xue, G.; Fiedler, A. T.; Martinho, M.; Münck, E.; Que, L., Jr. *Proc. Natl. Acad. Sci. U.S.A.* **2008**, *105*, 20615−20620.
(9) Kodera, M.; Itoh, M.; Kano, K.; Funabiki, T.; Reglier, M. *Angew. Chem., Int. Ed.* **2005**, *44*, 7104−7106.
(10) Dong, Y.; Zang, Y.; Shu, L.; Wilkinson, E. C.; Que, L., Jr.; Kauffmann, K.; Münck, E. *J. Am. Chem. Soc.* **1997**, *119*, 12683−12684.
(11) Kim, K.; Lippard, S. J. *J. Am. Chem. Soc.* **1996**, *118*, 4914−4915.
(12) Kodera, M.; Itoh, M.; Kano, K.; Funabiki, T. *Bull. Chem. Soc. Jpn.* **2006**, *79*, 252−261.
(13) Costas, M.; Mehn, M. P.; Jensen, M. P.; Que, L., Jr. *Chem. Rev.* **2004**, *104*, 939−986.
(14) Lee, S. K.; Fox, B. G.; Froland, W. A.; Lipscomb, J. D.; Münck, E. *J. Am. Chem. Soc.* **1993**, *115*, 6450−6451.
(15) Valentine, A. M.; Tavares, P.; Pereira, A. S.; Davydov, R.; Krebs, C.; Hoffman, B. M.; Edmondson, D. E.; Huynh, B. H.; Lippard, S. J. *J. Am. Chem. Soc.* **1998**, *120*, 2190−2191.
(16) England, J.; Martinho, M.; Farquhar, E. R.; Frisch, J. R.; Bominaar, E. L.; Münck, E.; Que, L., Jr. *Angew. Chem., Int. Ed.* **2009**, *48*, 3622−3626.
(17) Lacy, D. C.; Gupta, R.; Stone, K. L.; Greaves, J.; Ziller, J. W.; Hendrich, M. P.; Borovik, A. S. *J. Am. Chem. Soc.* **2010**, *132*, 12188−12190.
(18) England, J.; Guo, Y.; Van Heuvelen, K. M.; Cranswick, M. A.; Rohde, G. T.; Bominaar, E. L.; Münck, E.; Que, L., Jr. *J. Am. Chem. Soc.* **2011**, *133*, 11880−11883.
(19) Bigi, J. P.; Harman, W. H.; Lassalle-Kaiser, B.; Robles, D. M.; Stich, T. A.; Yano, J.; Britt, R. D.; Chang, C. J. *J. Am. Chem. Soc.* **2012**, *134*, 1536−1542.
(20) Oertling, W. A.; Kean, R. T.; Wever, R.; Babcock, G. T. *Inorg. Chem.* **1990**, *29*, 2633−2645.
(21) Czarnecki, K.; Kincaid, J. R.; Fujii, H. *J. Am. Chem. Soc.* **1999**, *121*, 7953−7954.
(22) Sastri, C. V.; Park, M. J.; Ohta, T.; Jackson, T. A.; Stubna, A.; Seo, M. S.; Lee, J.; Kim, J.; Kitagawa, T.; Münck, E.; Que, L., Jr.; Nam, W. *J. Am. Chem. Soc.* **2005**, *127*, 12494−12495.
(23) Lee, Y.-M.; Dhuri, S. N.; Sawant, S. C.; Cho, J.; Kubo, M.; Ogura, T.; Fukuzumi, S.; Nam, W. *Angew. Chem., Int. Ed.* **2009**, *48*, 1803−1806.
(24) Zheng, H.; Yoo, S. J.; Münck, E.; Que, L., Jr. *J. Am. Chem. Soc.* **2000**, *122*, 3789−3790.
(25) Zhang, X.; Furutachi, H.; Fujinami, S.; Nagatomo, S.; Maeda, Y.; Watanabe, Y.; Kitagawa, T.; Suzuki, M. *J. Am. Chem. Soc.* **2005**, *127*, 826−827.
(26) Yamashita, M.; Furutachi, H.; Tosha, T.; Fujinami, S.; Saito, W.; Maeda, Y.; Takahashi, K.; Tanaka, K.; Kitagawa, T.; Suzuki, M. *J. Am. Chem. Soc.* **2007**, *129*, 2−3.
(27) Fiedler, A. T.; Shan, X.; Mehn, M. P.; Kaizer, J.; Torelli, S.; Frisch, J. R.; Kodera, M.; Que, L., Jr. *J. Phys. Chem. A* **2008**, *112*, 13037−13044.
(28) Chavez, F. A.; Ho, R. Y. N.; Pink, M.; Young, V. G., Jr.; Kryatov, S. V.; Rybak-Akimova, E. V.; Andres, H.; Münck, E.; Que, L., Jr.; Tolman, W. B. *Angew. Chem., Int. Ed.* **2002**, *41*, 149−152.
(29) Kodera, M.; Shimakoshi, H.; Nishimura, M.; Okawa, H.; Iijima, S.; Kano, K. *Inorg. Chem.* **1996**, *35*, 4967−4973.
(30) Sanders-Loer, J.; Wheeler, W. D.; Shiemke, A. K.; Averill, B. A.; Loer, T. M. *J. Am. Chem. Soc.* **1989**, *111*, 8084−8093.
(31) Tshuva, E. Y.; Lippard, S. J. *Chem. Rev.* **2004**, *104*, 987−1012.
(32) Murray, L. J.; Lippard, S. J. *Acc. Chem. Res.* **2007**, *40*, 466−474.
(33) Seo, M. S.; Kim, N. H.; Cho, K.-B.; So, J. E.; Park, S. K.; Clémancey, M.; Garcia-Serres, R.; Latour, J.-M.; Shaik, S.; Nam, W. *Chem. Sci.* **2011**, *2*, 1039−1045.
(34) Kurtz, D. M., Jr. *Chem. Rev.* **1990**, *90*, 585−606.
(35) Noodleman, L.; Lovell, T.; Han, W.-G.; Li, J.; Himo, F. *Chem. Rev.* **2004**, *104*, 459−508.